Arch. Metall. Mater. **67** (2022), 4, 1325-1332

DOI: https://doi.org/10.24425/amm.2022.141058

JAMAL ARBAOUI[1,2*], JÉRÉMIE AUCHER[1], MOUSSA GOMINA[1], JOEL BREARD[1]

INVESTIGATION OF THERMAL AND MECHANICAL PROPERTIES OF THREE-DIMENSIONAL BRAIDED COMPOSITE MATERIALS

This paper investigates the thermal and mechanical properties of a composite made from a combination of 2063-epoxy resin and three different braided carbon-fiber fabric reinforcements. These fibres consist of HTS carbon, HTS carbon braided with nickel coated carbon and HTS carbon braided with nickel coated copper, respectively. The composites were manufactured through resin transfer molding (RTM) route. The thermal diffusivity of carbon fibers composites was measured at different temperature by using a flash method. The transverse and planar thermal conductivities were determined by measuring the specific heat, density and thermal diffusivities, respectively. The current research highlights the influence of adding nickel coated carbon and nickel-plated copper wires on the braided composites. The evaluation shows that the HTS carbon braided manufactured with nickel-plated copper wires presents higher in-plane thermal conductivity (in direction parallel of the fibres) when comparing to HTS carbon and HTS carbon braided manufactured with nickel coated carbon. The thermal conductivity benefits of those composite were achieved at the expenses of lower mechanical properties of braided composites investigated.

Keywords: Braided composites; thermal conductivity; bending; tensile

1. Introduction

Carbon fabric reinforced polymeric composites have been used extensively in numerous applications (i.e. automotive, ground transport, civil infrastructure, maritime and sport industries) [1,2]. Specifically, these composites are manufactured for components as flaps, aileron, landing-gear doors, and other artifacts used in aeronautical industry. The increase use of composites for various applications emphasizes its importance/significance related to superior thermal property in the above engineering system.

Thermal properties of composite materials depend on the amount and configuration of constituent materials. Generally, the fibers and matrices have different thermal properties. In these materials the carbon fibers have higher thermal conductivity than polymeric matrices ((e.g. 24.0 W/(m·K) for carbon fibers and 0.17-0.79 W/(m·K) for epoxy matrices)). There, fiber orientation, configuration, and volume fraction are factors that may affect the heat propagation in composite parts. Composites may present high thermal anisotropy in along-fiber and perpendicular-to-fiber direction. Based on Hwan-Boh Shim et al. [3], the thermal conductivity ratio between the two directions can vary between 40~130 W/(m·K). In practice, the in-plane direction of fiber-composite is aligned with the along-fiber direction, and through-thickness direction is perpendicular-to-fiber direction. In many applications, both in-plane heat spreading, and through-thickness heat removal are important for effective heat dissipation. The thermal conduction behaviour of an isotropic matrix reinforced with cylindrically orthotropic fibers is fully characterized by the values of its in-plane and through-thickness thermal conductivity [4]. A few researchers used LFA Micro Flash technique to measure the thermal properties of composite materials. Joven et al. [5] analysed the thermal conductivity and thermal diffusivity of carbon fiber-epoxy composites containing different fiber weave configurations by the means of LFA Micro Flash method. The NETZSCH LFA Micro Flash complies with the latest technology for modern laser flash systems. The table-top instrument allows measurements from –125°C to 1100°C using two different user-exchangeable furnaces. This instrument can be used for small and large sample sizes of up to 25.4 mm diameter and, with the integrated sample changer, measurements can be conducted simultaneously on several samples at the same time. Other scientists have [6-7-8] also employed LFA Micro Flash technique to

[1] LABORATOIRE CRISMAT, UMR 6508 CNRS/ENSICAEN, 6 BD MARÉCHAL JUIN, 14050 CAEN CEDEX 4, FRANCE
[2] UNIVERSITY OF CADI AYYAD, NATIONAL SCHOOL OF APPLIED SCIENCES, LABORATORY OF MATERIALS, PROCESSES, ENVIRONMENT AND QUALITY, B.P. 63, 46000, SAFI, MOROCCO

* Corresponding author: jamal57010@yahoo.fr

© 2022. The Author(s). This is an open-access article distributed under the terms of the Creative Commons Attribution-NonCommercial License (CC BY-NC 4.0, https://creativecommons.org/licenses/by-nc/4.0/deed.en which permits the use, redistribution of the material in any medium or format, transforming and building upon the material, provided that the article is properly cited, the use is noncommercial, and no modifications or adaptations are made.

estimate the thermal properties of composite materials. Braided composites are being widely used in the areas of aeronautics because of their superior mechanics and physics properties. In the early research considerable attention has focused on microstructure [9-10], stiffness [11-12] and strength [13], but investigations into thermal conductivity property of braided composites were very scare. In ref. [14], they investigated thermal conductivity property of 3-D braided composites using experimental tests. Schuster et al. [15] studied the effect of a three-dimensional fiber reinforcement on the out-of-plane which affect the thermal conductivity of composite materials. Liu et al. [16] and Li et al. [17] predicted the thermal conductivity of the 3D four-directional and five-directional braided composites based on different finite element models, respectively. Cheng et al. [18] investigated the thermal property of the 3D braided composites by experiment and numerical methods. Also, the effects of the braiding angle and fiber volume fraction on the thermal conductivity of the 3D braided composites have been assessed by Jiang et al. [19].

The mechanical properties of braided composites dependents greatly on their microstructure, which is much different from that of traditional composites. Accordingly, the braided composites can be tailored to meet some specific requirements from their applications. Braided composites are a novel class of composites with high performances. However, in the literature were noted that only few researches have studied the mechanical properties of some braided composites. Yau et al. [20] have studied the flexural and axial compressive failures of three-dimensionally braided composite. We have observed that the relationship of stress and strain presented linear characteristics when 3D braided I-beam appeared the initial damage using four-point flexure tests. Sun et al. [21] found that the compression deformation of 3D four-directional braided composites became more obvious with the increase of strain rate. Calme et al. [22] studied the static behaviour of 3D braided composite rings subjected to lateral compression. Li et al. [23] observed that the cutting edge on the thickness of 3D braided composite reduced the bending modulus. Also, the effect of braid angle on the flexural performance of structural braided thermoplastic composite beams have been assessed by Singh et al. [24].

In this study, the thermal conductivity of carbon fiber-epoxy composites was characterized using an LFA MicroFlash method. Thermal conductivity of these materials was evaluated using measurements of density, thermal diffusivity and specific heat. Samples manufactured with three braided composites (HTS carbon/2063, HTS carbon with carbon-coated nickel/2063 and HTS carbon with nickel-plated copper/2063) were analysed. The influence of carbon-coated nickel and nickel-plated copper on both in-plane and through-thickness thermal conductivities was identified. Uniaxial tensile testing of these braided composite materials was then conducted. Also, the three-point bending test were conducted on these composite materials to determine the flexural stress, flexural strain and Young modulus. The goal of this research was to provide a detailed experimental state of art for three braided composites which can act as a data base for the design and engineering application, especially aerospace components.

2. Experimental

2.1. Materials

2063-epoxy resin was used as matrix and supplied by Axon Technologies. The specification of the epoxy resin is shown in TABLE 1. Three different braided carbon fabric were used and supplied by Toho Tenax. They were HTS carbon braided, HTS carbon manufactured with carbon-coated nickel and HTS carbon manufactured with nickel-plated copper. The braided composite materials used in our experiment were provided by DJP composites and were manufactured for aeronautic applications. The composites studied are very consistent in terms of thickness that is about 2.4 mm (Fig. 1). The properties of HTS carbon fiber, nickel and copper are shown in TABLE 2.

TABLE 1

Properties of 2063 epoxy resin

Epoxy resin	Properties	Value
2063	Density (g cm^{-3})	1.16
	Cure cycle	80°C for 2 h and 180°C for 4 h
	Tg (°C)	180
	Thermal conductivity (W/mK)	0.17

TABLE 2

Properties of HTS carbon fiber, nickel and copper

	Properties	Value
HTS carbon fiber	Density (g cm^{-3})	1.80
	Thermal conductivity (W/mK)	10.00
Nickel	Density	8.90
	Thermal Conductivity (W/mK)	91.00
Copper	Density	8.92
	Thermal Conductivity (W/mK)	386.00

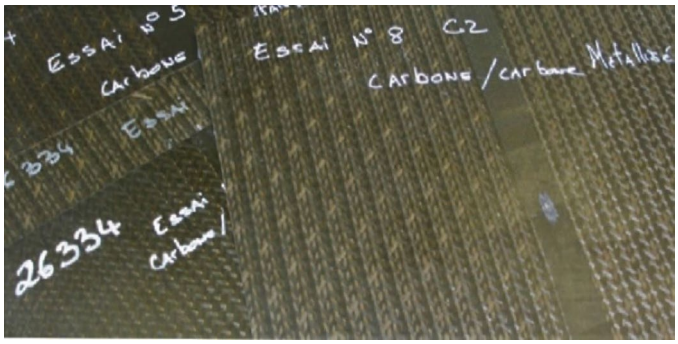

Fig. 1. Schematic configuration of composites studied

Triaxial-braided fabric that was evaluated in this study has basically three sets of yarns: braid (bias) and warp (axial). Braided yarns intertwine with each other around the axial yarns at about a 45° angle, whereas axial yarns lie throughout in the structure. Therefore, the triaxial-braided fabric is formed as shown in Fig. 2. In concept, unit cell (also known as representa-

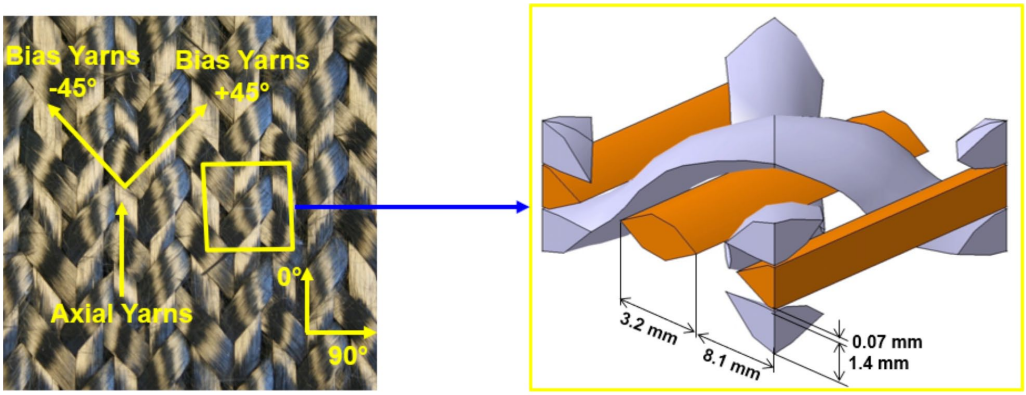

(a) Fabric Preform **(b) Unit Cell**

Fig. 2. Triaxial braided composite (a) fabric preform and (b) unit cell

tive volume element) assumes that there is a basic geometric pattern in the structure that represents the full-scale model. It can be seen from Fig. 2 that there is a specific repeated pattern of the tows in the structure. The same repeating pattern could be observed in all type of braids. Thus, each braided structure can be discretized in a number of identical repeating unit cells. Because of this periodic nature the behavior of the unit cell is same as that of the complete structure. For this reason, a single unit cell can simulate the entire braid structure provided that the correct boundary conditions are applied.

2.2. Thermal diffusivity and conductivity analysis

The thermal properties were measured using a light flash analyzer (LFA 457 Micro Flash TM system by NETZSCH-Gerätebau GmbH, Selb / Germany). This analyzer employ a xenon flash light which generate a pulse of energy on the bottom side of the sample. This pulse increases the sample temperature while the indium antimonide (InSb) infrared detector permits to measure the response time produced by the pulse of energy on the top side of the sample. This response time was utilized to calculate the thermal diffusivity. For instance, Parker/adiabatic method (ideal case) allows to calculate the thermal diffusivity as follows [25].

$$\alpha = 0.13879 \cdot \frac{l^2}{t_{1/2}} \tag{1}$$

where $t_{1/2}$ is half of the response time, l is the thickness, and a is the thermal diffusivity. Then, the thermal conductivity $\lambda(T)$ was calculated by multiplying $\alpha(T)$, specific heat $C_p(T)$, and sample density, $\rho(T)$:

$$\lambda(T) = \rho(T) \times C_p(T) \times \alpha(T) \tag{2}$$

2.3. Density analysis

The density versus temperature relationship was described by the change in the volume due to the thermal expansion. For a cubic unit cell of a material, the mass at room temperature is calculated as [26]:

$$m_0 = \rho_0 \times 1 \text{ cm}^3 \tag{3}$$

And the temperature T is deduced using the mass:

$$m(T) = \rho(T) \times v(T) = \\ = \rho(T) \times (1 + \eta(T))^3 \approx \rho(T) \times (1 + 3\eta(T)) \tag{4}$$

where, $\eta(T)$ is the coefficient of thermal expansion (unit of $\eta(T)$ is (1/K))

Assuming that the mass is preserved, the density can be expressed as:

$$\rho(T) = \frac{\rho_0}{1 + 3\eta(T)} \approx \rho_0 \times \left(1 - \eta(T)\right) \tag{5}$$

Because $\eta(T)$ for the studied composite materials is negligible being the order of 10^{-6} (1/K) we can obtain:

$$\rho(T) \approx \rho_0 \tag{6}$$

A pycnometer is used to accurately determine the bulk volume as part of apparent density determination. The system is filled with helium. The volume of each section of the system is known. The pressure is measured, before and after, for a section when atmospheric pressure is added. The ideal gas law is used to determine the volume of a specimen. The mass is measured separately, and by combining the volume and mass information, we get the apparent density such as apparent density = mass/volume.

2.4. Determination of fibre volume content

Accurate determination of the volume fraction of different components in a composite is essential to understand the overall thermal and mechanical performance of the composite material. Thermogravimetric analysis (TGA) instrument NETZSCH STA 449 F3 Jupiter® analyzer was used to characterize the fibre content of the carbon fibre/epoxy composites. By considering 20-30 mg of content of composites from a random chosen part we can measure accurately the TG. The specimens for TGA

were placed in a platinum crucible. They were heated in air atmosphere using high-resolution mode at low heating rates (20°C/min), which provided good basis for the determination of mass fractions. The strategy for establishing the fibre volume fraction consists of measuring the mass fraction of carbon fiber in the composite using thermal gravimetric analysis (TGA). By measuring the density of pure epoxy sample and composite one is possible to compute the fibre volume as the volume not occupied by the epoxy resin. The volume fraction of fibres (V_f) is given by:

$$V_f = \frac{M_f}{M_f + \left(\frac{\rho_f}{\rho_m}\right) M_m} \tag{7}$$

where M_f and M_m are the mass fractions of fiber and matrix, respectively, ρ_f and ρ_m are the densities of the fiber and matrix, respectively).

2.5. Specific heat (Cp)

Specific heat measurements were performed using differential scanning calorimetry (NETZSCH STA 449 F3 Jupiter® analyzer). The temperature was maintained in the range of 25°C to 1000°C at a heating rate of 20°C/min, under air atmosphere. The differential calorimetric allows to determine the glass transition temperatures (*Tg*) and degradation as well as the specific heat (*Cp*).

2.6. Tensile test

The tensile tests were conducted according to ISO 725-1B. Tensile properties were evaluated using an Instron 1342 mechanical tester with 100 kN capacity. The reproducibility of the results was achieved by testing five specimens for each compound. A crosshead displacement rate of 1 mm/min was used. The specimens tested for each type of braided composites are bounded by the following dimensions: length = 250 mm; width = 25 mm; and thickness = 2.4 mm, respectively. A typical tensile test and sample were reproduced in Fig. 3. The ultimate strength of composite was calculated using Eq. (8), where *F* and *S* are the applied force at breaking point and cross-sectional area of the coupon gauge section respectively. Ultimate strain was measured using an extensometer combined with the composite tensile stress in Eq. (9) which yield the Young's modulus.

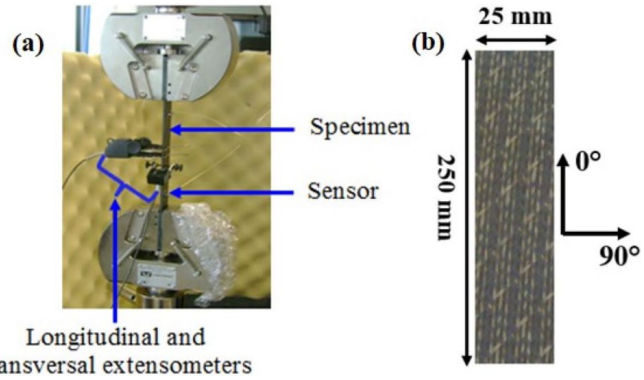

Fig. 3. Tensile testing machine (a) and sample dimensions (b)

$$\sigma = \frac{F_r}{S} \tag{8}$$

$$E = \frac{\sigma}{\varepsilon} \tag{9}$$

2.6. Bending test

Three-point bending testing is done to evaluated the flexural stress, and flexural strain of the composite materials. The 3-point bending test was carried out in an Instron Testing Machine in CRISMAT laboratoty, ENSICaen. The applied velocity of the bending load was 1 mm/min. A 2.4 mm thickness, 13.2 mm width and 100 mm length of strip was cut from the rectangular composite plate with the help of electrical power saw. Fig. 4 shows the load configuration for a beam subjected to three-point bending test. There, *F* is the load, *b* is the width of the specimen, *h* is the thickness of the specimen and *L* is the span (*L* = 80 mm). The flexural stress, flexural strain and Young's modulus are computed by the following equation 10, 11 and 12, respectively:

$$\sigma_f = \frac{3FL}{2bh^2} \tag{10}$$

$$\varepsilon_f = \frac{6h\delta_{\max}}{L^2} \times 100 \tag{11}$$

$$E = \left(\frac{F}{\delta}\right)\left(\frac{L}{h}\right)^3 \frac{1}{4b} \tag{12}$$

here $\delta_{\max}$ is maximal displacement and F/δ is the Slope (load-displacement curves).

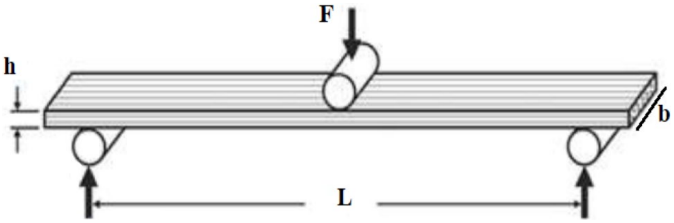

Fig. 4. Load configuration for a beam in three point bending

3. Results and discussion

3.1. Density and fibre volume content

Density was measured at room temperature for the different composites by using the Pycnometry method (Accu Pyc 1330). The experiments indicated that the different manufacturing braid

configurations generate various density. It is because the samples made of braids (HTS carbon braided manufactured with nickel coated copper /2063 and HTS carbon braided with nickel coated carbon/2063) showed higher values than those measured in braid HTS carbon samples. This is explained by the great density of copper and nickel compared to the density of carbon fiber. Once the density was determined at room temperature, in the next step were measured the volume fraction of different composites by using a TGA in order to obtain the mass fractions of fibers. Typical decomposition curve of 2063-epoxy and HTS carbon-fiber are shown in Fig. 5, where two-step degradation process for the composites studied can be seen. The first step weight loss processes occurred roughly at 380-410°C, which corresponds to degradation of the resin epoxy. The second step happened from about 700°C to 750°C. This step may be assigned to the decomposition of the carbon fiber. Having obtained the mass fraction of the composites, were determined the fiber volume fractions using Equation (5). The density and fibre volume content of different fibers used in this study are listed in TABLE 3.

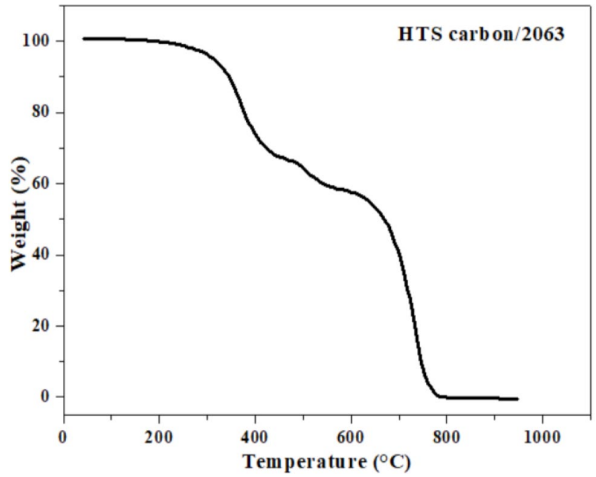

Fig. 5. The thermogravimetric analysis (TGA) analysis of HTS Carbon/2063 composite

TABLE 3

Density, fiber weight and volume content of three different composites

Sample	Density (g cm^{-3})	Fiber weight (%)	Fiber volume (%)
HTS carbon/2063	1.56	70	60
HTS carbon + CNi/2063	1.66	33.5% HTS	32% HTS
		36.5% CNi	24% CNi
HTS carbon + CoNi/2063	1.77	29.6% HTS	37% HTS
		41.4% CoNi	8% CoNi

3.2. Specific heat capacity

Specific heat capacity is an important parameter for thermal conductivity calculation and was obtained by DSC analysis. The evolution of the specific heat versus temperature is presented in Fig. 6. Overall, tests indicated that Cp curves were similar for all samples and changed proportionally to temperature. For instance,

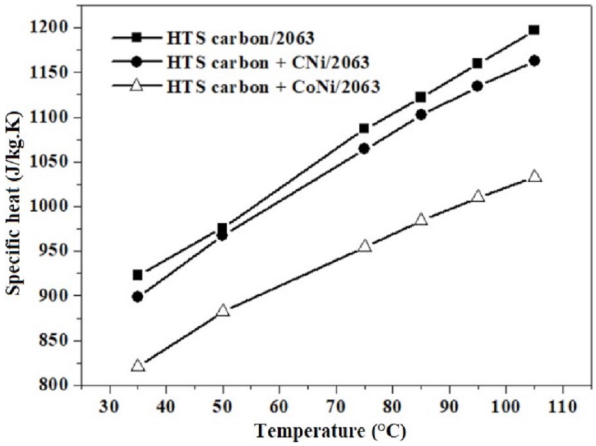

Fig. 6. Transverse thermal conductivity of three braided composites

Cp values at temperature (35°C) were around 925 J/(kg·K) while those at 110°C were 1200 J/(kg·K) for the HTS carbon/2063 system tested. Furthermore, Cp increased linearly proportional to temperature for all the samples. It is observed that the specific heat of HTS carbon braided with nickel coated copper /2063 showed lower values than those compared by braid HTS carbon/2063 and HTS carbon braided with nickel coated carbon/2063 samples. This can be explained by the low specific heat of copper (385 J/kg·K) when compared by the specific heat of nickel (444 J/(kg·K)) and carbon fiber (712 J/(kg·K)).

3.3. Thermal diffusivity and conductivity

The thermal diffusivity was determined in the temperature range 25-80°C, on ~ 8 mm × 8 mm × 2 mm parallelepiped-shaped specimens. The measurement of the in-plane thermal diffusivity is performed on ~ 9 mm × 6 mm × 2 mm rectangular-stacked specimens in the directions parallel and perpendicular of the carbon fibers. Thermal conductivity was calculated using Equation 2. The transverse conductivity versus the temperature is shown in Fig. 7. It is visible that the transverse conductivity of

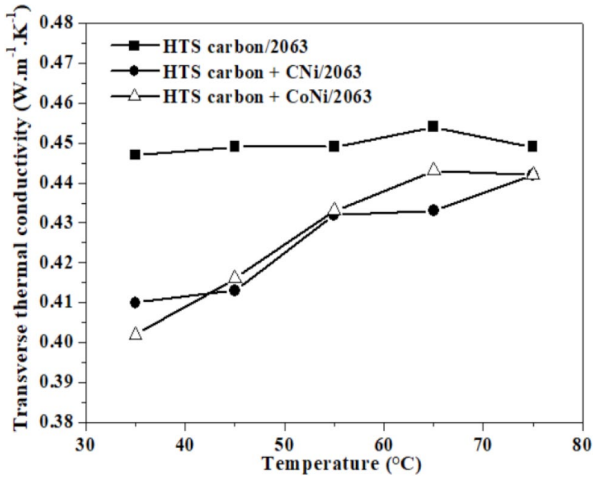

Fig. 7. In-plane thermal conductivity in the direction parallel to the fibers of three braided composites

the HTS carbon/2063 is higher than the HTS carbon + CNi/2063 and HTS carbon + CoNi/2063. The Figs. 8 and 9 shows the evolution of the in-plane thermal conductivity for in parallel and perpendicular of fibers direction of braided composites. The in-plane thermal conductivity of the braided composite was higher as compared to the transverse thermal conductivity. We found that the in-plane thermal conductivity in the direction parallel to the fibres of the HTS carbon + CoNi/ 2063 composites reach a higher value when compared to HTS carbon/2063 and HTS carbon + CNi/2063 composites. This can be explained by great thermal conductivity of copper in relation with thermal conductivity of nickel and carbon fiber. Also, we do not observed a big difference for the in-plane thermal conductivity and the direction perpendicular to the fibers for the three composites studied. These experimental results confirm that the transverse and in-plane thermal conductivity in the direction perpendicular to the fibers is less affected by adding the carbon-coated nickel and nickel-plated copper wires. On the other hand, in-plane thermal conductivity in the direction parallel to the fibers is higher which is influenced more by adding the nickel-plated copper wires than by adding the carbon-coated nickel.

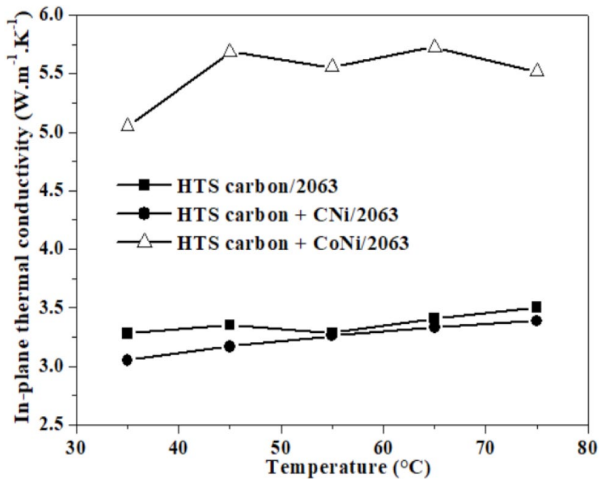

Fig. 8. In-plane thermal conductivity in the direction perpendicular to the fibers of three braided composites as a function of temperature

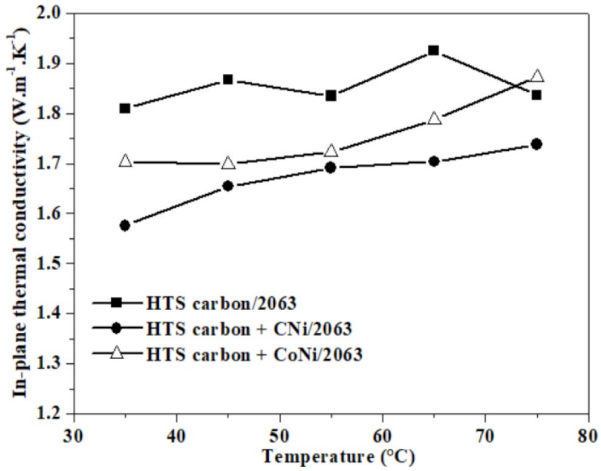

Fig. 9. Stress-strain curves of three braided composites in the perpendicular to the fiber direction

3.4. Tensile test

The mechanical properties of the three material systems were experimentally determined in a series of tensile tests. Test panels were fabricated and machined to permit direct determination of the materials performance in both the longitudinal direction (parallel to the 0° yarns) and the transverse direction (perpendicular to the 0° yarns (90°)). The principal Young's moduli, ultimate strain and the ultimate tensile strengths were measured in these tests.

The tensile behaviour in the transverse direction (perpendicular to the 0° yarns) is shown in Fig. 10. The results can be described in three principal phases: the first phase is initial linear elastic behaviour followed by a phase of non-linear one in which the maximum loading is reached. In the last phase, it is observed the total rupture of the samples. Obviously, the test pieces have undergone plastic deformation. Fig. 11 depicts the stress-strain curve for three braided composites solicited in the longitudinal direction (parallel to the 0° yarns). Here, the materials do not show the plastic behaviour and rupture occurs in the elastic range, demonstrating the brittle behaviour.

Results of the mechanical properties of these composites are summarized in TABLE 4. The table contains the average

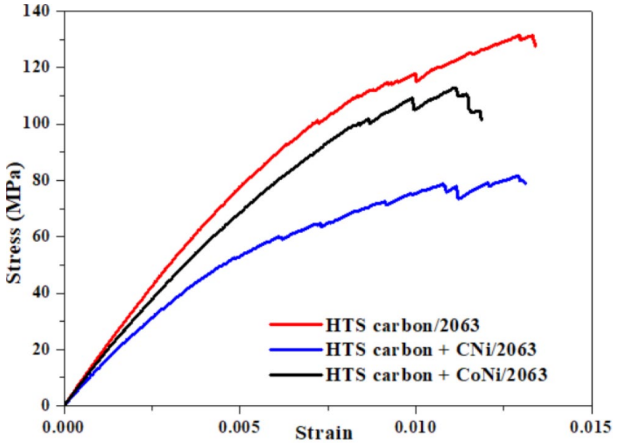

Fig. 10. Stress-strain curves of three braided composites in the parallel to the fiber direction

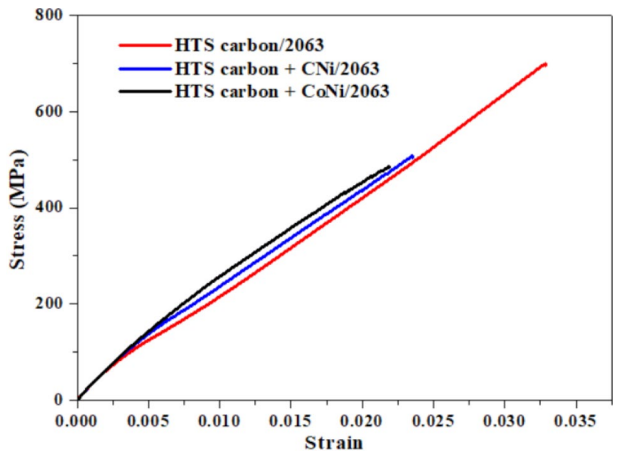

Fig. 11. Typical load-displacement curves of of three braided composites

strengths, Young's modulus and ultimate strains (as recorded by the extensometer) for the longitudinal (direction of 0° yarns) and transverse (perpendicular to the 0° yarns) tension tests. Longitudinal strengths and young's modulus were greater than transverse strengths and young's modulus for all three materials. In fact, transverse strengths and Young's modulus showed little sensitivity to fiber architecture. The longitudinal strengths and young's modulus showed a range of values, however. For example, the HTS carbon + CoNi/2063 braided composite specimens' longitudinal strength was 76% greater than their transverse strength. The HTS carbon/2063 specimens, by comparison, were 81% stronger in the longitudinal direction than they were in the transverse direction. Also, the ultimate strength and the Young's modulus of the HTS carbon/2063 braided composite is higher as compared to the other composites. These results show that the ultimate strength changes when is added 24% of the carbon coated copper and 8% of the nickel-plated copper, respectively.

TABLE 4

The tensile properties of three braided composites in the parallel and perpendicular to the fiber direction

Sample	Orientation	Young's modulus (GPa)	Ultimate strength (MPa)	Ultimate strain (%)
HTS carbon/2063	0°	54.98	677.82	1.24
	90°	17.60	129.42	1.37
HTS carbon + CNi/2063	0°	58.02	501.99	0.87
	90°	13.86	84.85	1.38
HTS carbon + CoNi/2063	0°	40.62	453.24	1.31
	90°	15.50	109.96	1.39

3.4. Bending test

Fig. 12 depict the load-displacement curve of the braided composites solicited in three-point bending. The bending behavior presents similar trend and can be described in three principal phases: the first phase reveals an initial linear elastic behavior followed by a phase of nonlinear one in which the maximum loading is reached. In the last phase, a reduction in the load applied is observed until the total rupture of the sample occurs. This figure shows also a decrease of the maximum load and bending stiffness with adding the 24% of the carbon coated copper and 8% of the nickel-plated copper, respectively. From this figure, the flexural stress, flexural strain and Young's modulus have been obtained and listed in TABLE 5. By adding 24% of carbon coated copper is produced a decrease of flexural stress and bending stiffness by about 19% and 5%, respectively. Also, by adding 8% of nickel-plated copper is induced a reduction of flexural stress and bending stiffness by about 38% and 46%, respectively.

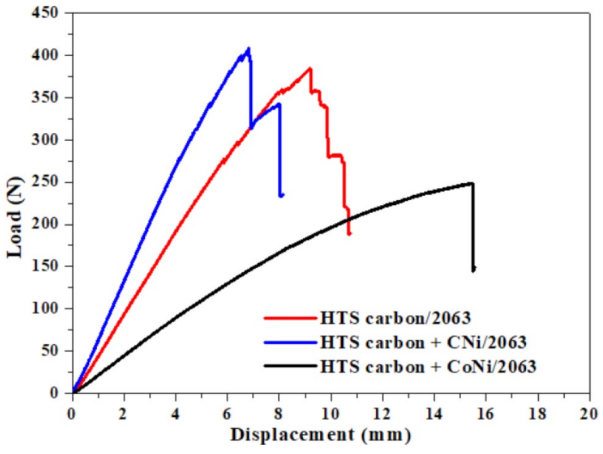

Fig. 12. The specific heat of three braided composites

TABLE 5

The bending properties of three braided composites in the parallel and perpendicular to the fiber direction

Sample	Flexural stress (MPa)	Young's modulus (MPa)	Flexural strain (%)
HTS carbon/2063	769.96 ± 34	47.78 ± 6	1.78 ± 0.09
HTS carbon + CNi/2063	622.80 ± 47	45.25 ± 5	1.48 ± 0.12
HTS carbon + CoNi/2063	472.38 ± 82	25.67 ± 3	2.59 ± 0.50

4. Conclusion

A detailed experimental investigation was conducted to analyse the mechanical and thermal properties of three braided composites. These materials were prepared with HTS carbon/2063, HTS carbon braid manufactured with carbon-coated nickel/2063 and HTS carbon braid manufactured with nickel-plated copper/2063. The results showed better in-plane thermal conductivity compared to transverse thermal conductivity in the temperature range of 25-80°C. The HTS carbon braid containing nickel-plated copper wires with 2063 epoxy resin have higher values of in-plane thermal conductivity in the direction parallel to the fibres as compared to the other studied composites at the same temperature range.

The results showed superior tensile properties in terms of higher tensile strength and elastic modulus for braided composites solicited in along-fiber direction. However, by adding either carbon coated copper or nickel-plated copper a slightly reduction of flexural stress and bending stiffness is produced.

Acknowledgements

This work is a part of the THERMELEC project. It is supported by the DGE through the ASTECH competitiveness cluster, in which several partners are collaborating (Région Basse-Normandie, Company Hispano-Suiza, Dassault Aviation, DJP, MADEP, LI2C, INRETS, SERAM, LEG, CNRT Matériaux Caen).

REFERENCES

[1] F.U. Buehler, J.C. Seferis, Compos. Part A. Appl. Sci. Manuf. **31**, 741-748 (2000).

[2] B.S. Hayes, E.N. Gilbert, J.C. Seferis, Compos. Part A. Appl. Sci. Manuf. **31**, 717-725 (2000).

[3] H.B. Shim, M.K. Seo, S.J. Park, J. Mater. Sci. **37**, 1881-1885 (2002).

[4] D.P.H. Hasselman, H.K.Y. Donaladson, J.R.J. Thomas. J. Compos. Mater. **27**, 637-644 (1993).

[5] J. Ronald, M. Bob, J. Compos. Mater. **52**, 4075-4085 (2018).

[6] S. Min, J. Blumm, A. Lindemann, Thermochim. Acta. **455**, 46-49 (2007).

[7] A. Veillère, H. Kurita, A. Kawasaki, Y. Lu, J.M. Heintz, J.F. Silvain, Mat. **12**, 4030 (2019).

[8] W. Keji, C. Jingpeng, M. Zhenyong, H. Qiongqiong, T. Jingyu, Energ. Fuel **31**, 7052-7059 (2017).

[9] L. Chen, X. M. Tao, C.L. Choy, Compos. Sc. Technol. **59**, 391-404 (1999).

[10] D.L. Wu, Compos. Sc. Technol. **56**, 225-233 (1996).

[11] Z.G. Liu, M. Lu, H.C. Mai, Journal of Beijing University of Aeronautics and Astronautics **26**, 182-185 (2000).

[12] Z.G. Liu, Z.X. Lu, M. Lu, Acta. Mat. Compos. Sin. **17**, 66-69 (2000).

[13] Z.X. Lu, Z.G. Liu, H.C. Mai, Journal of Beijing University of Aeronautics and Astronautics **28**, 563-565 (2002).

[14] Y. Gowayed, J.C. Hwang, Compos. Eng. **5**, 1177-1186 (1994).

[15] J. Schuster, D. Heider, K. Sharp, M. Glowania, Mech. Compos. Mater. **45**, 165-174 (2009).

[16] Z.G. Liu, H.G. Zhang, Z.X. Lu, D.S. Li, Chin. J. Aeronaut. **20**, 327-331 (2007).

[17] D.S. Li, X.Z. Lu, Z.G. Liu, Z.P. Li, Compos. **23**, 1455-1460 (2008).

[18] W. Cheng, S.G. Zhao, Z.G. Liu, Acta. Aeronaut. Astronaut. Sin. **23**, 102-105 (2002).

[19] L.L. Jiang, G. Xu, S. Cheng, X. Lu, T. Zeng, Compos. Struct. **108**, 578-583 (2014).

[20] S.S. Yau, T.W. Chou, F.K. Ko, Compos. **17**, 227-32 (1986).

[21] B. Sun, L. Yang, B. Gu, Aiaa J. **43**, 994-999 (2005)

[22] O. Calme, D. Bigaud, P. Hamelin, Compos. Sci. Technol. **56**, 95-106 (2005).

[23] J.L. Li, Y. Jiao, Y. Sun, L.M. Wei, Mater. Des. **28**, 2417-2424 (2007).

[24] A. Singh, N. Reynolds, E.M. Keating, A.E. Barnett, S.K. Barbour, D.J. Hughes, Compos. Struct. **261**, 1-14 (2021)

[25] W.J. Parker, R.J. Jenkins, C.P. Butler, G.L. Abbott J. Appl. Phys. **32**, 1679-1684 (1961).

[26] C. Benaqqa, M. Gomina, M.A. Beurotte, M. Boussuge, B. Delattre, K. Pajot, E. Pawlak, F. Rodrigues, Appl. Therm. Eng. **62**, 599-606 (2014).